RSC Advances

RSC Publishing

COMMUNICATION

Flexible hierarchical nanocomposites based on MnO_2 nanowires/CoAl hydrotalcite/carbon fibers for high-performance supercapacitors†

Cite this: *RSC Advances*, 2013, **3**, 1045

Received 18th October 2012,
Accepted 16th November 2012

DOI: 10.1039/c2ra22566b

www.rsc.org/advances

Jingwen Zhao, Zhenzhi Lu, Mingfei Shao, Dongpeng Yan, Min Wei,* David G. Evans and Xue Duan

A hierarchical nanocomposite based on MnO_2 nanowire/CoAl layered double hydroxide/carbon fibers is fabricated by a facile two-step method as a high-performance supercapacitor. The CoAl-LDH nanocrystals grown on flexible carbon fibers were prepared *via* an *in situ* hydrothermal method, followed by loading of MnO_2 nanowires through a direct redox reaction between the Co^{2+} species and MnO_4^-. The hierarchical MnO_2/LDH/CFs electrode as a supercapacitor displays a high specific capacitance (944 F g^{-1} at 1 A g^{-1}) and rate capability, good stability and excellent long-term cycling life.

To meet the urgent need for sustainable and renewable power sources, in modern electronic industries many efforts have been made in developing flexible, lightweight and environmentally friendly energy storage devices.[1,2] Electrochemical capacitors, also known as supercapacitors,[3] are the most promising candidates for various portable systems and automotive applications owing to their high power density, excellent pulse charge–discharge characteristics and long cycle life.[4–6] Pseudocapacitive transition-metal oxides, MnO_2 for instance, have been extensively used in supercapacitors due to their high capacitance, low cost and environment-friendliness.[7,8] Given that the poor conductivity of MnO_2 (10^{-5}–10^{-6} S cm^{-1}) limits the charge–discharge rate for high-power applications,[9,10] further efforts have been directed at incorporating MnO_2 nanostructures with carbon-based materials or conductive polymers.[11–14] Another problem of MnO_2 materials arises from the dense packing and inaccessible surface area as a high loading is applied, which leads to a remarkable increase in contact resistance and the resulting decrease in specific capacitance. Therefore, taking into account the efficient utilization of the pseudocapacitance of MnO_2, it is highly essential to achieve a hierarchical morphology and reliable electric connection for the purpose of obtaining high-performance MnO_2-based supercapacitors.

Recent efforts have been devoted to exploring composite pseudocapacitive materials, such as binary metal oxides/hydroxides[15,16] and mixed metal oxides[17,18] by combining the unique properties of individual constituents. It was reported that the synergistic effect between different compositions can be achieved through suitable micro-/nanostructure design.[19,20] Therefore, more advanced and complex heterostructures have been fabricated to improve the pseudocapacitive performance, such as core–shell structures,[21,22] tube-structured arrays,[23–25] coaxial nanowires[26] and conductive carbon/polymer supported metal oxides/hydroxides composites.[27–32] It is believed that an ideal electrode material consists of a three-dimensional (3D) interpenetrating network of electron and ion pathways for efficient mass/electron transport.[33–35] A key challenge in this direction is to develop a desirable electrode architecture that favors sufficient exposure of the electroactive species for the Faradaic redox reaction, and simultaneously enhance the kinetics of ion/electron transport throughout the electrode. Based on the above consideration, one promising route is to rationally design and construct the hybridization of pseudocapacitive oxides/hydroxides with sophisticated nanoarchitectures, which provides a highly-accessible surface area, fast ion diffusion and excellent electronic conductivity.

Herein, we demonstrate the design and fabrication of a novel nanocomposite (MnO_2/LDH/CFs) by loading MnO_2 nanowires onto CoAl layered double hydroxide (LDH) nanowalls grown on flexible carbon fibers (CFs) for high-performance supercapacitors. The single-crystalline LDH with a highly accessible surface area serves uniquely as a reductant and the framework for anchoring the MnO_2 nanowires simultaneously. Both LDH and MnO_2 are employed as the active species, which contribute to the total specific capacitance; while the conductive CFs with appropriate channels guarantee effective electron/ion transport throughout the electrode. By virtue of the synergetic contribution from individual constituents and the sophisticated configuration, the resulting MnO_2/LDH/CFs composite exhibits a highly boosted specific

State Key Laboratory of Chemical Resource Engineering, Beijing University of Chemical Technology, Beijing 100029, P. R. China.
E-mail: weimin@mail.buct.edu.cn; Fax: 86-10-64425385; Tel: 86-10-64412131

† Electronic Supplementary Information (ESI) available: Experimental procedures, gas adsorption/desorption analysis, XRD patterns and additional electrochemical data are included. See DOI: 10.1039/c2ra22566b

Scheme 1 Schematic illustration for the fabrication of MnO_2/LDH/CFs nanocomposite as high-performance supercapacitor.

capacitance, superior to its single-component samples (LDH/CFs and MnO_2/CFs). In addition, this integrated electrode manifests a remarkable rate capability and excellent long-term cycling stability. Therefore, the control over the multi-composition and bottom-up architecture demonstrated in this work offers a promising strategy for the fabrication of supercapacitor materials used in electrochemical energy storage.

Our strategy is schematically shown in Scheme 1. The preparation process of the MnO_2/LDH/CFs composite mainly involves (i) growing vertically-aligned LDH nanowalls on the CFs by a facile hydrothermal process and (ii) anchoring the MnO_2 nanowires on the LDH/CFs scaffold *via* an *in situ* spontaneous redox reaction between the Co^{2+} species within LDH and potassium permanganate ($KMnO_4$) in solution (see the detailed preparation procedure in the ESI†). Carbon fiber is significantly advantageous as a current collector and support of pseudocapacitive materials in lightweight supercapacitor towards portable and transport applications.[36] Fig. 1a shows the typical SEM and optical images of the primary CFs used in this study; the well-interconnected CFs with a rather smooth surface with a diameter of ~7.5 μm provide an electrically conductive network. The SEM image of the as-prepared LDH/CFs (Fig. 1b) displays a high density and uniform coating covering the skeletons of the CFs. The corresponding X-ray energy dispersive spectroscopy (EDS) spectra (Fig. 1b, inset) demonstrates the presence of cobalt, aluminum and oxygen elements in the coating, with a Co/Al molar ratio of 1.97, in line with the nominal ratio (Co : Al = 2 : 1). Fig. 1c shows a single carbon fiber coated with integrated nanowalls standing perpendicularly while intersecting each other, creating a highly open and porous structure. The thickness of one single LDH platelet is estimated to be ~10 nm (Fig. 1c, inset). The fabrication of the LDH nanowalls can significantly enlarge the specific surface area from 1.875 $m^2 g^{-1}$ for bare CFs to 12.102 $m^2 g^{-1}$ for LDH/CFs (Fig. S1†). A typical TEM image (Fig. 1d) displays the thin hexagonal morphology of a single LDH nanocrystal; the corresponding selected area electron diffraction (SAED) pattern (Fig. 1d, inset) exhibits hexagonally arranged spots, indicating the high crystallinity of the LDH nanowalls (its XRD pattern is shown in Fig. S2†).

The vertically-aligned and cross-linked LDH nanowalls grown on the CFs can serve as a robust and conductive scaffold for the loading of an additional pseudoactive material. The controlled deposition of MnO_2 onto the hierarchical LDH/CFs was amazingly triggered by simply immersing the LDH/CFs sample into a $KMnO_4$ aqueous solution at room temperature without stirring; a spontaneous redox reaction occurs between the Co^{2+} in LDH

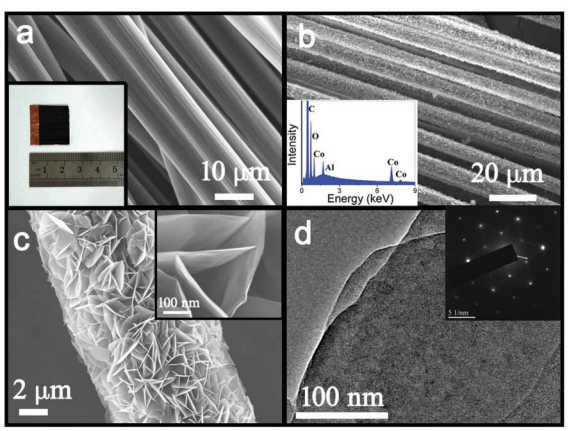

Fig. 1 (a) SEM and optical (the inset) images of the CFs; SEM images of the LDH/CFs at (b) low magnification (inset: the corresponding EDS results) and (c) high magnification (inset: the enlarged image); (d) TEM image of an individual LDH nanocrystal grown on the CFs (inset: the corresponding SAED pattern).

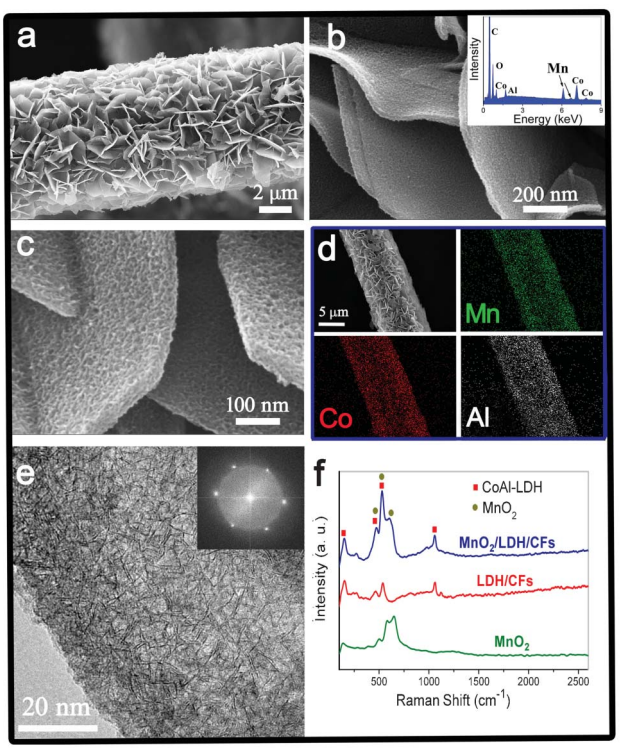

Fig. 2 (a–c) SEM images of the MnO_2/LDH/CFs heteronanostructure (inset of Fig. 2b: the corresponding EDS results) and (d) EDS mapping results from a single MnO_2/LDH/CFs structure; (e) TEM image of an individual MnO_2/LDH composite (inset: the corresponding FFT pattern); (f) Raman spectra of MnO_2, LDH/CFs and MnO_2/LDH/CFs.

and MnO_4^- in solution. As can be seen from the SEM images (Fig. 2a–c), a uniform and dense MnO_2 nanowire coating was deposited onto the surface of the LDH nanowalls, resulting in a well-defined structure with sophisticated configuration. Elemental mapping in the scanning SEM mode (Fig. 2d) and the corresponding EDS pattern (Fig. 2b, inset) confirm a homogeneous distribution of a MnO_2 phase throughout the hierarchical structure. It was verified by BET measurements that the specific surface area of the LDH/CFs framework was further increased from 12.102 $m^2 g^{-1}$ to 37.836 $m^2 g^{-1}$ after coating with the MnO_2 layer (Fig. S1†). The resulting MnO_2/LDH/CFs heterostructure fabricated by the two-step strategy exhibits a fully-integrated structure in which the CFs provide a 3D backbone and the densely-packing LDH nanowalls serve as both a reductant and support for the homogeneous distribution of nanoscaled MnO_2.

Fig. 2e shows a typical TEM image of an individual MnO_2/LDH nanostructure, in which numerous MnO_2 nanowires, of ~0.8 nm in diameter, are finely-dispersed on the LDH support, introducing an additional interconnected porosity. The hexagonal diffraction in the corresponding fast Fourier transformation (FFT) pattern is attributed to the {1010} crystalline planes of the LDH phase (Fig. 2e, inset), indicative of the maintenance of the LDH structure upon the immobilization of MnO_2. No MnO_2-related diffraction pattern can be found, indicating the amorphous nature of the MnO_2 coating, which is further demonstrated by the XRD studies (Fig. S2†). It has been reported that amorphous MnO_2 is more favorable for supercapacitor applications compared with the crystalline MnO_2 coatings.[37,38] The Raman spectra are shown in Fig. 2f, further testifying the presence of the MnO_2 phase. The evolution of MnO_2 nanowires was examined by conducting a time-dependent growth method. SEM images clearly display a gradual enhancement both in particle size and coverage of MnO_2 nanowires along with the increase of deposition time (Fig. S3†; their CVs are shown in Fig. S4†). The sample with a deposition time of 120 min possesses the largest capacitance (mass ratio of MnO_2/LDH is 0.11), therefore it was chosen for further studies (Fig. S3f†).

Typical XPS spectra of LDH/CFs and MnO_2/LDH/CFs are shown in Fig. 3. For the sample of MnO_2/LDH/CFs, the peaks of Mn $2p_{3/2}$ and Mn $2p_{1/2}$ (Fig. 3A, curve b) are located at 642.1 and 653.9 eV respectively, with a spin energy separation of 11.8 eV, which is in good agreement with the reported data of Mn 2p states in MnO_2.[29,39] The Co 2p core lines of the LDH/CFs sample split into Co $2p_{3/2}$ (780.5 eV) and Co $2p_{1/2}$ (796.7 eV) peaks accompanied with two satellite bands at 785.5 and 802.1 eV (Fig. 3B, curve a), indicative of a high-spin Co^{2+} state in the LDH/CFs.[40] After the *in situ* deposition of the MnO_2 layer, both the Co $2p_{3/2}$ and Co $2p_{1/2}$ peaks shift to lower energy levels (779.9 and 796.2 eV, respectively), along with a slight decrease in the intensity of satellite bands (Fig. 3B, curve b). Such an observation indicates the occurrence of a partial valence change from Co^{2+} to Co^{3+},[41,42] implying that the driving force for the immobilization of MnO_2 arises from the redox reaction between MnO_4^- in solution and Co^{2+} in LDH phase. In this work, the integrated LDH/CFs network plays the roles of both a 3D support and reductant, ensuring the cleanness of the MnO_2/LDH interface without impurities. In addition, the specific structure of the LDH phase provides an ordered arrangement of Co^{2+} for a sufficient reduction of MnO_4^-,[43,44] imparting a good microenvironment for the nucleation and stabilization of MnO_2. Therefore, the facile spontaneous deposition strategy in this work affords the clean and well-dispersive MnO_2 nanowires anchoring to the LDH scaffold, combining unique properties of individual constituents.

The electrochemical tests were performed in a three-electrode electrochemical cell at room temperature with a Pt plate counter electrode and a Hg/HgO reference electrode in 1.0 M LiOH aqueous electrolyte. Fig. 4a shows the cyclic voltammograms (CVs) of the MnO_2/LDH/CFs electrode, in comparison with the samples of LDH/CFs and MnO_2/CFs (MnO_2 nanowires directly electrodeposited on CFs; Fig. S5†). The quasi-rectangular CV curve for the MnO_2/CFs electrode (green curve in Fig. 4a) is attributed to the reversible intercalation/de-intercalation processes of Li^+ from the electrolyte.[9,39] Given that the electrolyte penetration depth is approximately 20 nm, the ultrathin morphology of the LDH nanocrystals (~10 nm in platelet thickness) favors a high capacitance, by effectively shortening the proton diffusion distance.[45] Two pairs of redox peaks at ~0.2 and 0.55 V are clearly observed for the LDH/CFs electrode (red curve in Fig. 4a;

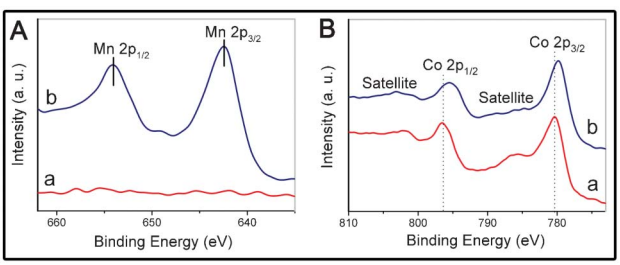

Fig. 3 XPS spectra of (A) Mn 2p and (B) Co 2p: (a) LDH/CFs and (b) MnO_2/LDH/CFs.

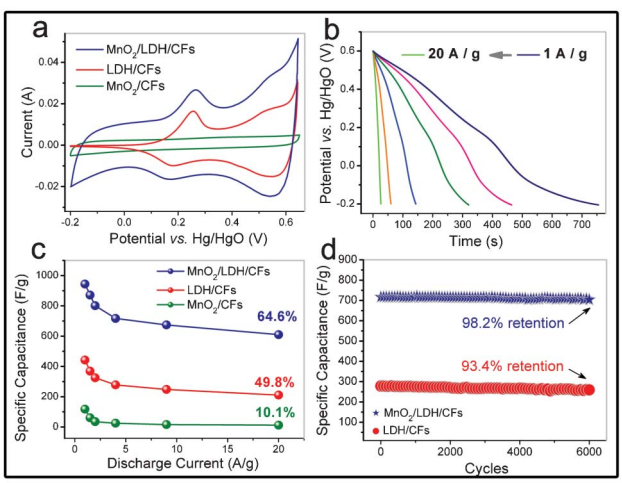

Fig. 4 (a) CVs of MnO_2/LDH/CFs, LDH/CFs and MnO_2/CFs electrodes at a scan rate of 20 mV s^{-1}; (b) Galvanostatic discharge curves of MnO_2/LDH/CFs at various discharge current densities; (c) the specific capacitance of MnO_2/LDH/CFs, LDH/CFs and MnO_2/CFs at various current densities; (d) cycling performance of the MnO_2/LDH/CFs and LDH/CFs (the specific mass loading is ~1.2 mg cm^{-2}).

Fig. S6†), which correspond to the reversible reactions of Co^{2+}/Co^{3+} and Co^{3+}/Co^{4+} associated with OH^-:[21,46]

$$Co(OH)_2 + OH^- \leftrightarrow CoOOH + H_2O + e^- \quad (1)$$

$$CoOOH + OH^- \leftrightarrow CoO_2 + H_2O + e^- \quad (2)$$

In the case of the MnO_2/LDH/CFs electrode, its CV curve displays four peaks which are all assigned to the LDH phase, with approximately rectangular shape and much higher currents than either single component (blue curve in Fig. 4a; Fig. S7†). This CV shape change is attributed to the introduction of amorphous MnO_2, which can afford an extra reversible intercalation/de-intercalation process of Li^+ from the electrolyte.[9,19,29] Since the contribution from the CFs to the capacitance is negligible (Fig. S8†), the total capacitance of the MnO_2/LDH/CFs sample originates from the redox pseudocapacitance of both the LDH and MnO_2 species, accounting for the largely enhanced charge storage capability.

A series of galvanostatic charge–discharge measurements were performed on the MnO_2/LDH/CFs electrode at various currents (Fig. 4b), from which the discharge curves exhibit a typical pseudocapacitive behavior, in accordance with its CV results. The obtained specific capacitances of the nanocomposite are 944, 871, 801, 717, 674 and 610 F g^{-1} at the current of 1, 1.5, 2, 4, 9 and 20 A g^{-1}, which are higher than those of many previous MnO_2-based conducting matrix compound electrodes[8,11–14] and hybrid pseudocapacitive materials.[19–21] Fig. 4c further displays the specific capacitances of the LDH/CFs, MnO_2/CFs and MnO_2/LDH/CFs electrodes as a function of the applied current density (their discharge curves at 1 A g^{-1} are shown in Fig. S9†). Within the whole current density range, the MnO_2/LDH/CFs electrode yields a substantially higher specific capacitance than that of the two comparison samples. For instance, the gravimetric capacitance reaches 944 F g^{-1} at a current density of 1 A g^{-1}, which is highly superior to that of the individual LDH/CFs (442 F g^{-1}) and MnO_2/CFs (118 F g^{-1}) samples. The capacitances of LDH/CFs and MnO_2/CFs decrease quickly as the charging–discharging rate increases from 1 to 20 A g^{-1}, *i.e.*, only 49.8% and 10.1% retentions can be obtained, respectively. In contrast, for the MnO_2/LDH/CFs electrode, 64.6% of the capacitance is maintained, indicating its superior rate capability for high power applications.

Another important requirement for supercapacitor applications is cycling capability. The cycling life tests for both the MnO_2/LDH/CFs and LDH/CFs electrode were carried out at 4 A g^{-1}, as shown in Fig. 4d. After 6000 charge–discharge cycles, the MnO_2/LDH/CFs electrode shows a 98.2% capacitance retention, much higher than that of the LDH/CFs sample (93.4% retention). This is further verified by the stable charge–discharge curves for the last 30 cycles (Fig. S10a†: with ~98.9% Coulombic efficiency). After long-term cycling, the structural integrity and hierarchical morphology of the MnO_2/LDH/CFs composite are overall preserved with no obvious deterioration (Fig. S10b†). In this respect, the MnO_2 nanowires are proposed to serve as a protection layer to maintain the structural integrity and prevent any significant collapse or disassembly during the harsh long-term reaction. To further highlight the superior electrochemical stability of the nanocomposite, the cycling performance was recorded at programmed current densities (Fig. S11†). The stepwise testing reveals that the MnO_2/LDH/CFs material can remain electrochemically stable even after exposure to sudden current changes. Furthermore, after storage of the MnO_2/LDH/CFs electrode in the electrolyte for one month, ~97.6% of the initial capacitance can still be maintained after another 850 cycles without a noticeable decrease. Additionally, six electrodes based on the MnO_2/LDH/CFs nanocomposite were fabricated independently under the same conditions, which show an acceptable reproducibility of the specific capacitance with an RSD of 2.1% (Fig. S12†). The results demonstrate the excellent supercapacitive capability of this hierarchical composite electrode, which meets the requirements of both high capacitance and long cycling life for high-performance energy storage devices.

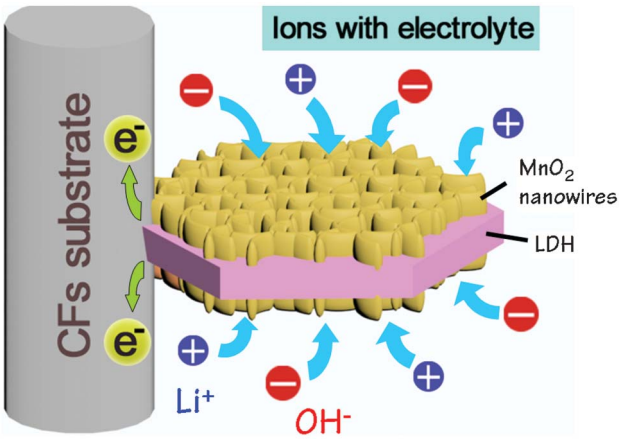

Scheme 2 Schematic representation of the energy storage mechanism for the MnO_2/LDH/CFs composite.

Based on the results above, it can be concluded that the rational combination of MnO_2 and LDH into a unique integrated architecture can substantially improve the electrochemical properties. The MnO_2/LDH/CFs structure and energy storage mechanism, taking advantage of the sophisticated 3D configuration and synergistic contribution from the individual species, are illustrated in Scheme 2. Firstly, by a spontaneous deposition method, the MnO_2 nanowires are well distributed onto the LDH nanowalls, forming an enlarged surface area and a hierarchically porous structure (Fig. S1†), which can minimize the solid-phase ion diffusion length and serve as "ion reservoirs" to steadily supply adequate OH^- and Li^+. This substantially guarantees the sufficient Faradaic reaction in both the internal LDH and external MnO_2 layer at high current densities. The electrochemical impedance spectroscopy results (Fig. S13†) also demonstrate that the MnO_2 coating leads to a significant decrease in charge–transfer resistance and ion diffusion resistance compared with the LDH/CFs sample, thus improving the electrochemical kinetics. Secondly, the as-grown LDH nanowalls for the loading of nanoscaled MnO_2 build up a 3D macroporous scaffold with an electrolyte-filled network, enhancing the ionic conductivity greatly and ensuring a high utilization of electrode material. Thirdly, the CFs backbone (current collector) with good electronic conductivity allows efficient charge transport of the composite. In addition, the

pore channels formed between the numerous long fibers provide an accessible ion percolation path, further facilitating the mass transport of electrolytes, which is critical to the high power density.

In summary, a facile, cost-effective and potentially scalable technique was developed to fabricate MnO_2/LDH/CFs electrodes for flexible supercapacitors. In this hierarchical structure, the 3D LDH nanowalls are coated with a MnO_2 nanowire shell by a direct redox reaction between LDH and MnO_4^-, offering a largely enhanced surface area and porous network. Owing to the synergistic effect of the active materials and the unique hierarchical structure, the resulting MnO_2/LDH/CFs composite electrode allows facilitated mass/electron transport and accordingly exhibits a large specific capacitance, good rate capability and excellent long-term cycle stability. The synthetic approach presented here can be extended for the fabrication of other multifunctional heterostructures by the use of one- and two-dimensional building units, which can be used as promising candidates in sensors, catalysis and energy storage devices.

This work was supported by the National Natural Science Foundation of China (NSFC) and the 973 Program (grant no. 2011CBA00504). M. Wei particularly appreciates the financial aid from the China National Funds for Distinguished Young Scientists of the NSFC.

References

1 M. Winter and R. J. Brodd, *Chem. Rev.*, 2004, **104**, 4245.
2 A. S.Arico, P. Bruce, B. Scrosati, T. -M. Tarascon and W. V. Schalkwijk, *Nat. Mater.*, 2005, **4**, 366.
3 P. J. Hall, M. Mirzaeian, S. I. Fletcher, F. B. Sillars, A. J. R. Rennie, G. O. Shitta-Bey, G. Wilson, A. Cruden and R. Carter, *Energy Environ. Sci.*, 2010, **3**, 1238.
4 P. Simon and Y. Gogotsi, *Nat. Mater.*, 2008, **7**, 845.
5 J. R. Miller and P. Simon, *Science*, 2008, **321**, 651.
6 T. Brezesinski, J. Wang, S. H. Tolbert and B. Dunn, *Nat. Mater.*, 2010, **9**, 146.
7 W. Deng, X. Ji, Q. Chen and C. E. Banks, *RSC Adv.*, 2011, **1**, 1171.
8 R. R. Salunkhe, K. Jang, S. Lee and J. Ahn, *RSC Adv.*, 2012, **2**, 3190.
9 D. Bélanger, T. Brousse and J. W. Long, *Electrochem. Soc. Interface*, 2008, **17**, 49.
10 X. Lang, A. Hirata, T. Fujita and M. Chen, *Nat. Nanotechnol.*, 2011, **6**, 232.
11 R. Liu and S. B. Lee, *J. Am. Chem. Soc.*, 2008, **130**, 2942.
12 H. Zhang, G. Cao, Z. Wang, Y. Yang, Z. Shi and Z. Gu, *Nano Lett.*, 2008, **8**, 2664.
13 X. Lu, T. Zhai, X. Zhang, Y. Shen, L. Yuan, B. Hu, L. Gong, J. Chen, Y. Gao, J. Zhou, Y. Tong and Z.-L. Wang, *Adv. Mater.*, 2012, **24**, 938.
14 S. W. Lee, J. Kim, S. Chen, P. T. Hammond and Y. Shao-Horn, *ACS Nano*, 2010, **4**, 3889.
15 M. Jayalakshmi and K. Balasubramanian, *J. Electrochem. Sci.*, 2008, **3**, 1196.
16 C.-C. Hu, C.-Y. Hung, K.-H. Chang and Y.-L. Yang, *J. Power Sources*, 2011, **196**, 847.
17 G.-Y. Zhao, C.-L. Xu and H.-L. Li, *J. Power Sources*, 2007, **163**, 1132.
18 J.-H. Kim, K. Zhu, Y. Yan, C. L. Perkins and A. J. Frank, *Nano Lett.*, 2010, **10**, 4099.
19 T.-Y. Wei, C.-H. Chen, H.-C. Chien, S.-Y. Lu and C.-C. Hu, *Adv. Mater.*, 2010, **22**, 347.
20 X. Xia, J. Tu, Y. Zhang, X. Wang, C. Gu, X. Zhao and H. J. Fan, *ACS Nano*, 2012, **6**, 5531.
21 C. Guan, J. Liu, C. Cheng, H. Li, X. Li, W. Zhou, H. Zhang and H. J. Fan, *Energy Environ. Sci.*, 2011, **4**, 4496.
22 J. Y. Kim, S. -H. Lee, Y. Yan, J. Oh and K. Zhu, *RSC Adv.*, 2012, **2**, 8281.
23 X. Lu, G. Wang, T. Zhai, M. Yu, J. Gan, Y. Tong and T. Li, *Nano Lett.*, 2012, **12**, 1690.
24 P. Banerjee, I. Perez, L. Henn-Lecordier, S. B. Lee and G. W. Rubloff, *Nat. Nanotechnol.*, 2009, **4**, 292.
25 Q. Li, Z.-L. Wang, G.-R. Li, R. Guo, L.-X. Ding and Y. -X. Tong, *Nano Lett.*, 2012, **12**, 3803.
26 A. L. M. Reddy, M. M. Shaijumon, S. R. Gowda and P. M. Ajayan, *Nano Lett.*, 2009, **9**, 1002.
27 L. Yuan, X.-H. Lu, X. Xiao, T. Zhai, J. Dai, F. Zhang, B. Hu, X. Wang, L. Gong, J. Chen, C. Hu, Y. Tong, J. Zhou and Z.-L. Wang, *ACS Nano*, 2012, **6**, 656.
28 Z. Tang, C. Tang and H. Gong, *Adv. Funct. Mater.*, 2012, **22**, 1272.
29 R. Liu, J. Duay and S. B. Lee, *ACS Nano*, 2010, **4**, 4299.
30 R. B. Rakhi, W. Chen, D. Cha and H. N. Alshareef, *Nano Lett.*, 2012, **12**, 2559.
31 Z. Chen, V. Augustyn, X. Jia, Q. Xiao, B. Dunn and Y. Lu, *ACS Nano*, 2012, **6**, 4319.
32 H. Wang, H. S. Casalongue, Y. Liang and H. Dai, *J. Am. Chem. Soc.*, 2010, **132**, 7472.
33 H. Zhang, X. Yu and P. V. Braun, *Nat. Nanotechnol.*, 2011, **6**, 277.
34 J. W. Long, B. Dunn, D. R. Rolison and H. S. White, *Chem. Rev.*, 2004, **104**, 4463.
35 K.-H. Chang, Y.-F. Lee, C.-C. Hu, C.-I. Chang, C.-L. Liu and Y.-L. Yang, *Chem. Commun.*, 2010, **46**, 7957.
36 X. J. Zhang and Z. M. Shen, *Fuel*, 2002, **81**, 2199.
37 H. Y. Lee and J. B. Goodenough, *J. Solid State Chem.*, 1999, **144**, 220.
38 S. B. Ma, K. Y. Ahn, E. S. Lee, K. H. Oh and K. B. Kim, *Carbon*, 2007, **45**, 375.
39 D. Liu, Q. Zhang, P. Xiao, B. B. Garcia, Q. Guo, R. Champion and G. Cao, *Chem. Mater.*, 2008, **20**, 1376.
40 T. J. Chuang, C. R. Brundle and D. W. Rice, *Surf. Sci.*, 1976, **59**, 413.
41 R. Ma, J. Liang, K. Takada and T. Sasaki, *J. Am. Chem. Soc.*, 2011, **133**, 613.
42 R. Xu and H. C. Zeng, *Chem. Mater.*, 2001, **13**, 297.
43 P. J. Sideris, U. G. Nielsen, Z. Gan and C. P. Grey, *Science*, 2008, **321**, 113.
44 A. I. Khan and D. O'Hare, *J. Mater. Chem.*, 2002, **12**, 3191.
45 C.-C. Hu, K.-H. Chang, M.-C. Lin and Y.-T. Wu, *Nano Lett.*, 2006, **6**, 2690.
46 C. Yuan, L. Yang, L. Hou, J. Li, Y. Sun, X. Zhang, L. Shen, X. Lu, S. Xiong and X. W. Lou, *Adv. Funct. Mater.*, 2012, **22**, 2560.